Gas Pixel Detectors

Ronaldo Bellazzini
INFN - Pisa

8th International Workshop on Radiation Imaging Detectors (IWORID-8)
Pisa 2-6/july 2006

Polarimetry: The Missing Piece of the Puzzle

Imaging: Chandra

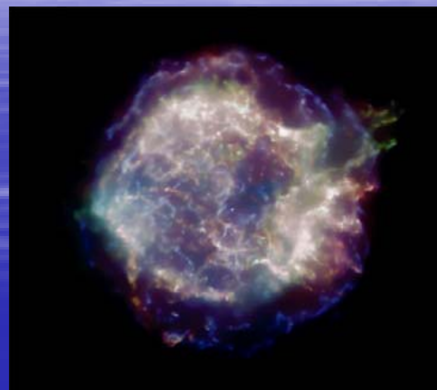

Timing: RXTE

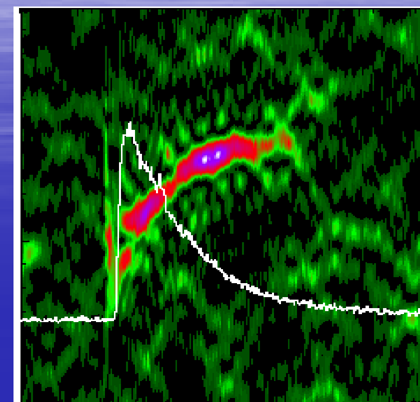

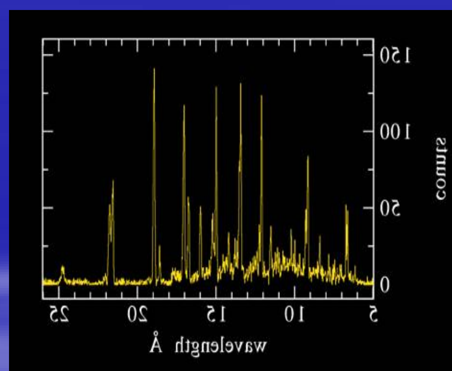

Spectroscopy: AstroE2, Constellation-X, Chandra

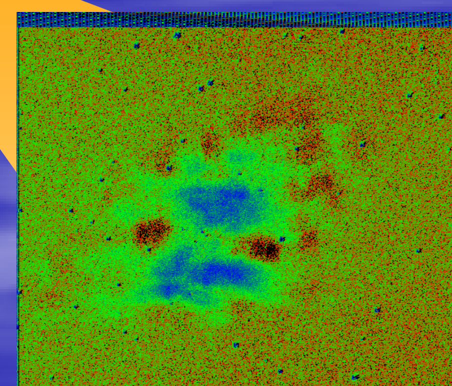

Polarimetry: ?

The only polarized source already known

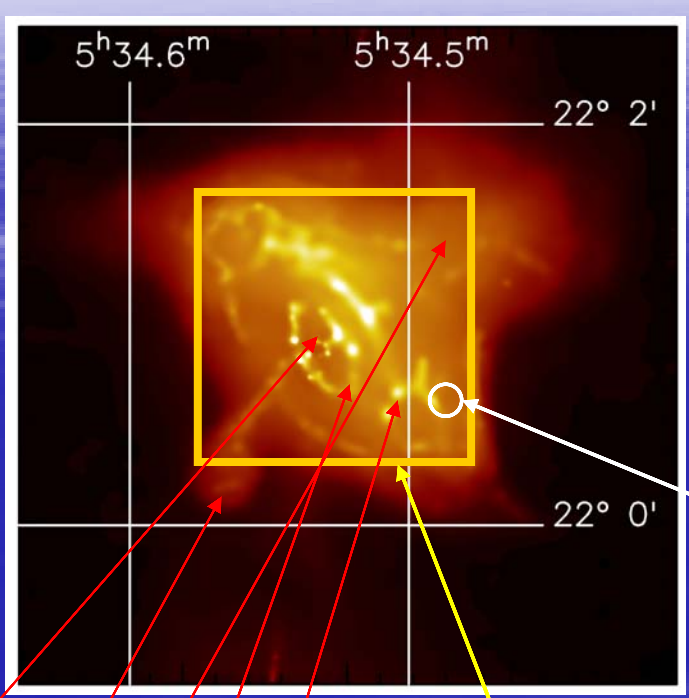

p.s.f.

PSR

NW jet

SE jet

Inner torus

Outer torus

f.o.v.

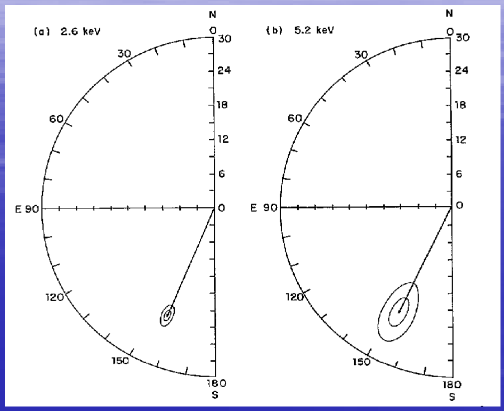

Positive measurement: of X-ray polarization of the Crab Nebula without pulsar contamination (by lunar occultation, Weisskopf et al., 1978).

P = 19.2 ± 1.0 %

θ = 156.4° ± 1.4°

But this is only the average measurement.The structure is much more complex!

With XPOL we can perform the separate polarimetry, imaging, spectroscopy and timing of details of the major structures

Photoelectric cross section

The photoelectric effect is very sensitive to photon polarization!

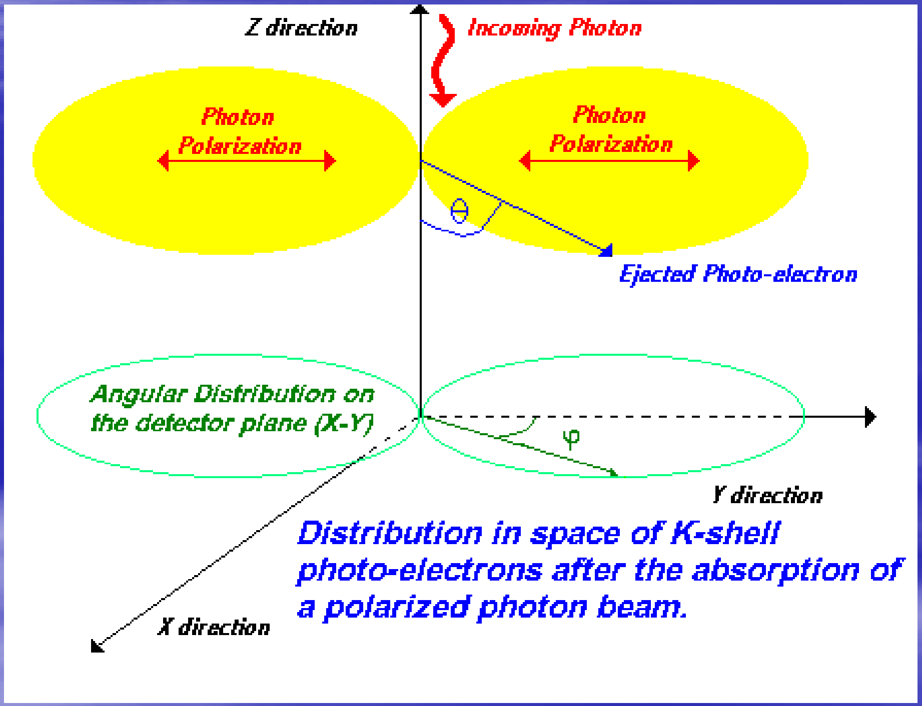

Simple analytical expression for photoemission differential cross section (k-shell photoelectron in non-relativistic limit):

$$\frac{\partial\sigma}{\partial\Omega} = r_o^2 \frac{Z^5}{137^4}\left(\frac{mc^2}{h\nu}\right)^{7/2} \frac{4\sqrt{2}\sin^2(\theta)\cos^2(\varphi)}{(1-\beta\cos(\theta))^4}$$

If we project on the plane orthogonal to the propagation direction…

$$\frac{\partial\sigma}{\partial\Omega} \propto \cos^2\phi$$

Photoelectron and Auger angular distributions

Photoelectron emission angular distributions

$$\frac{\partial\sigma}{\partial\theta} \propto \frac{\sin^3(\theta)}{(1-\beta\cos(\theta))^4}$$

$$\frac{\partial\sigma}{\partial\phi} \propto \cos^2\phi$$

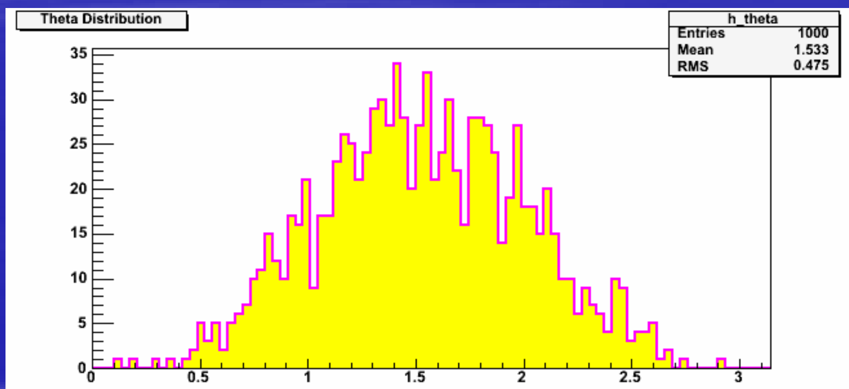

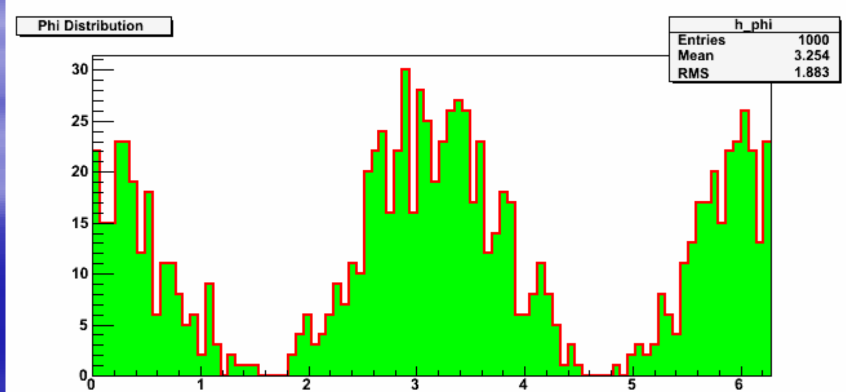

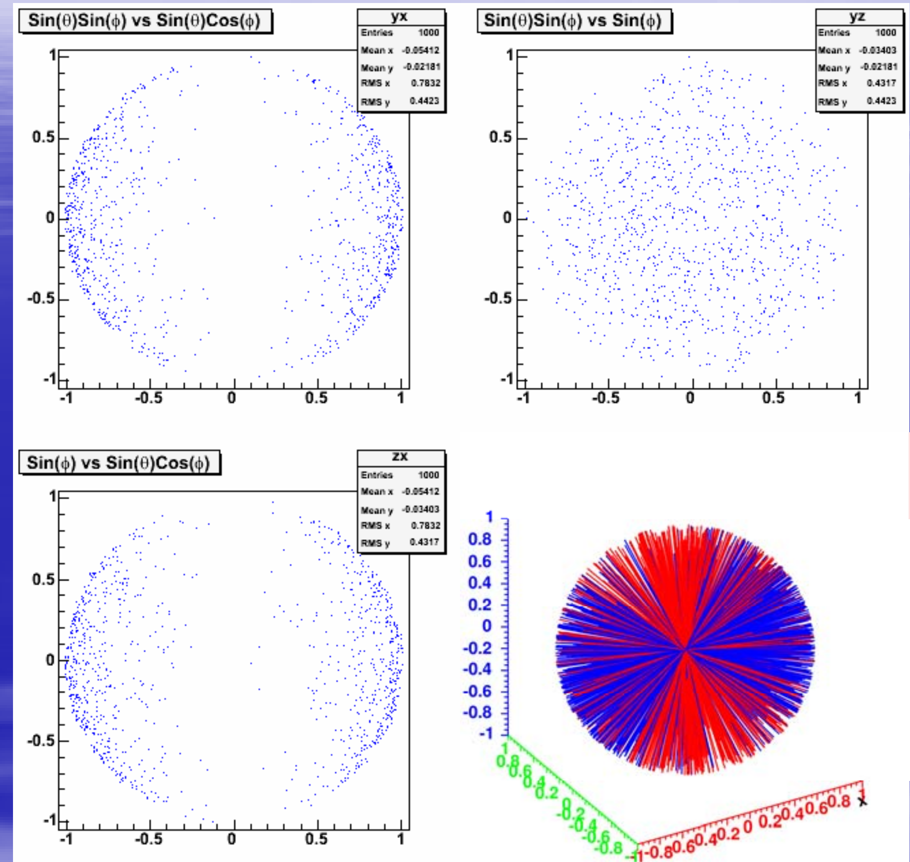

Auger emission directions

Photoelectron emission directions

The principle of detection

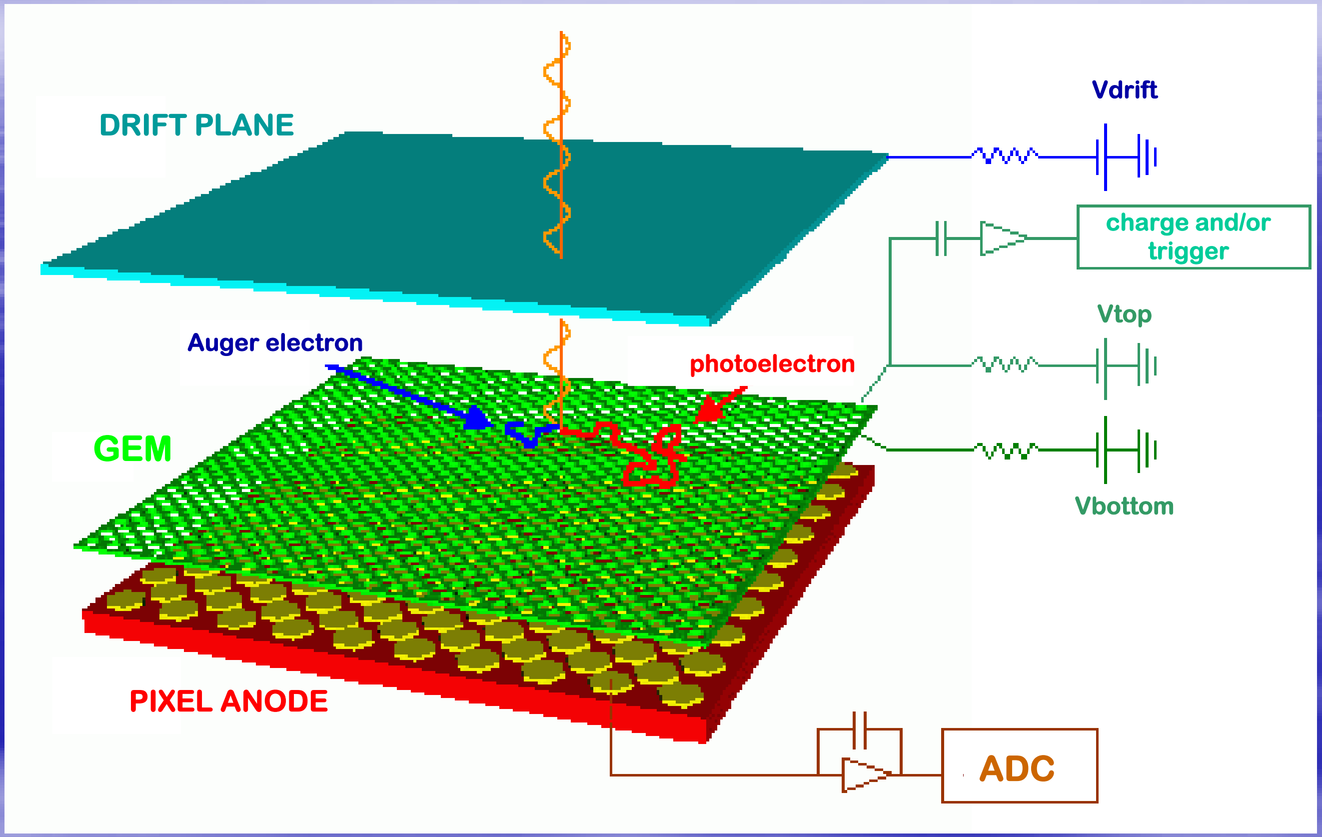

GEM electric field

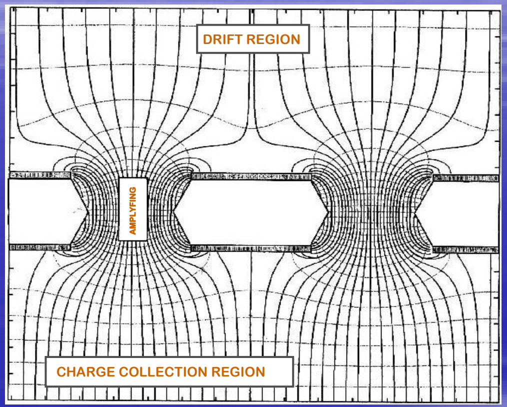

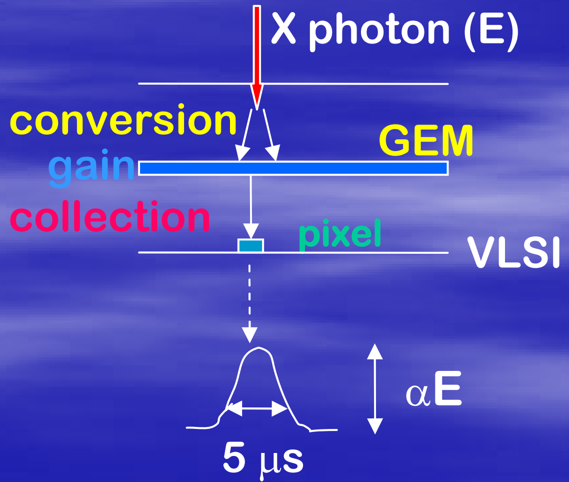

A custom CMOS analog chip is at the same time the pixelized charge collecting electrode and the amplifying, shaping and charge measuring front-end electronics of Micropattern Gas Detectors (MPGD) or other suitable charge multiplier

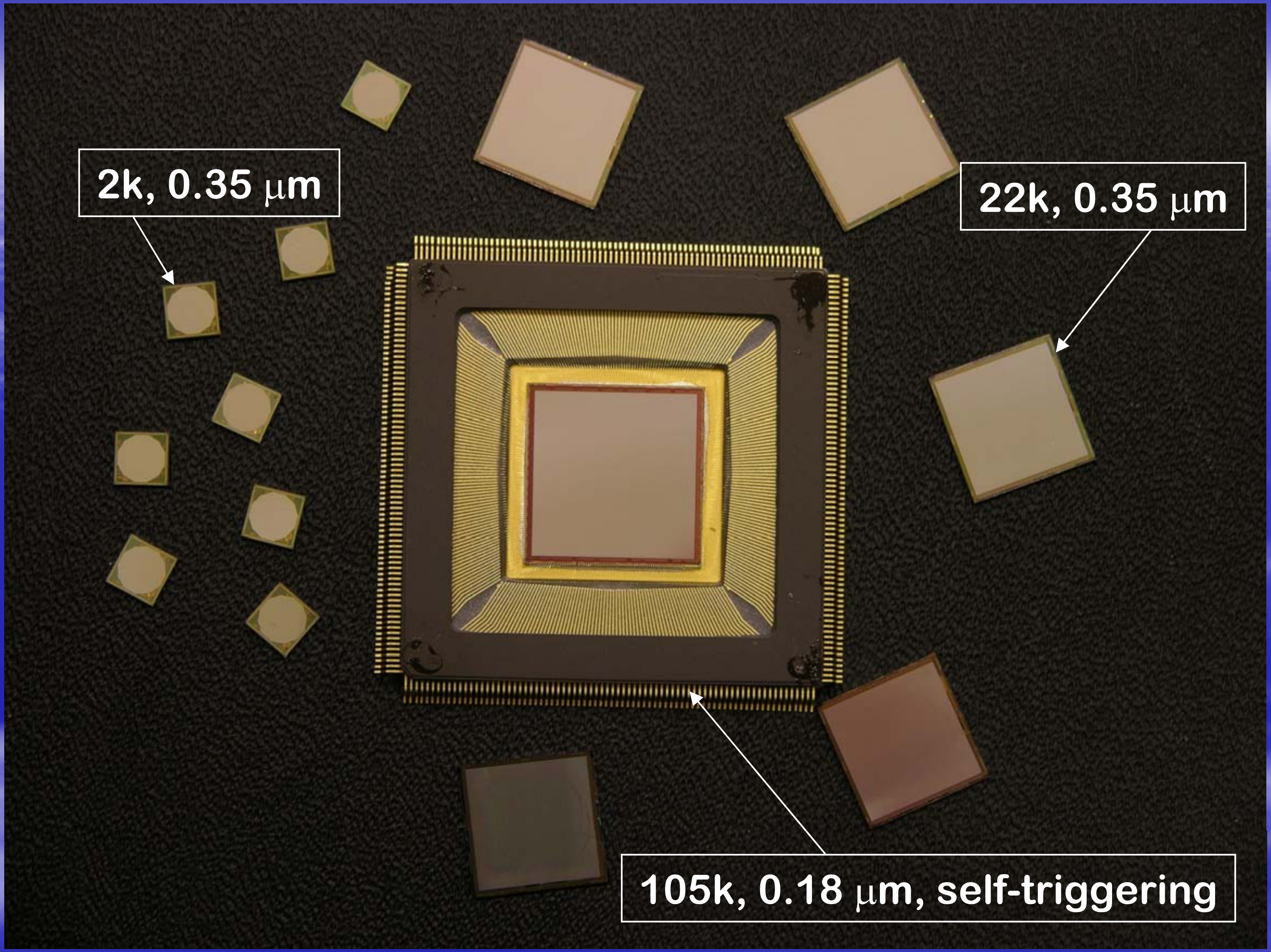

three ASIC generations of increasing size, reduced pitch and improved functionality have been realized

The collecting anode/read-out VLSI chip

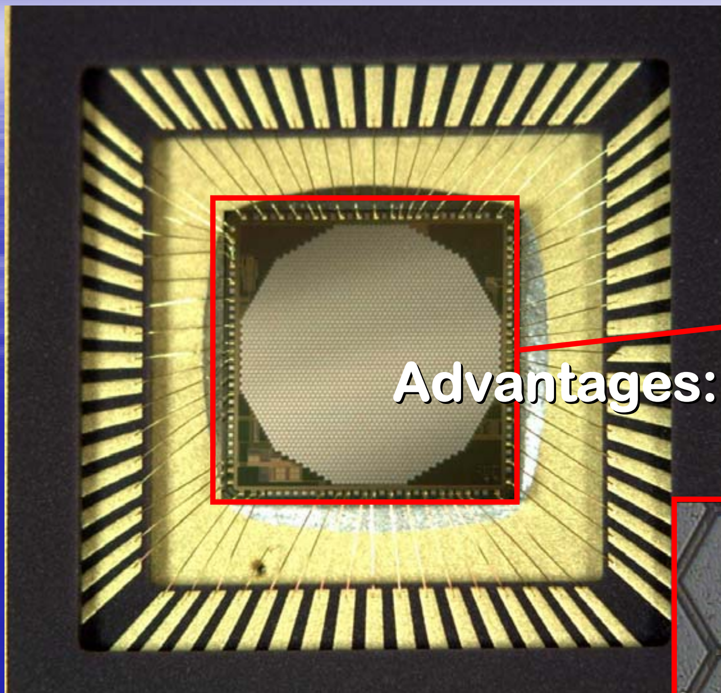

First ASIC prototype

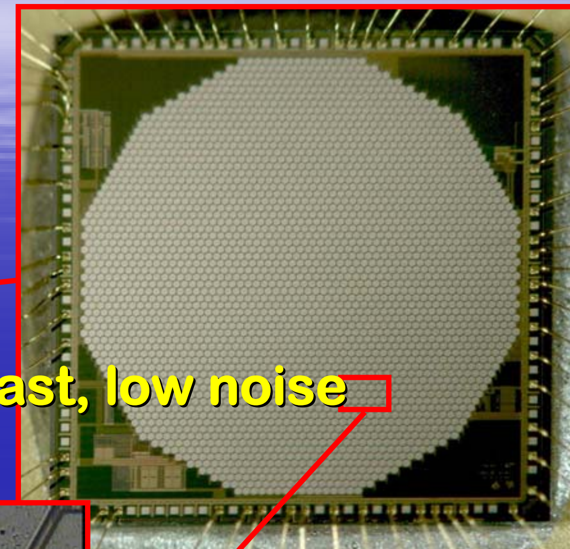

Advantages: asynchronous, fast, low noise

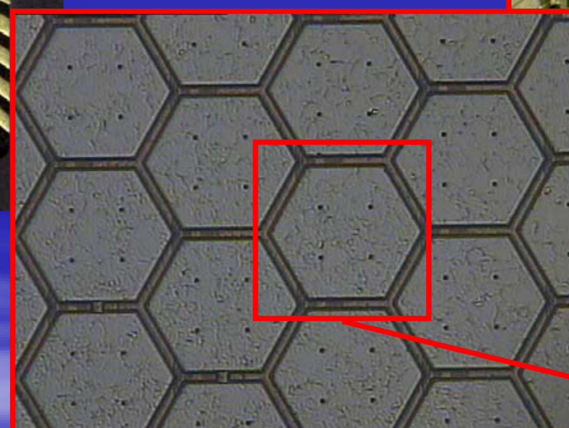

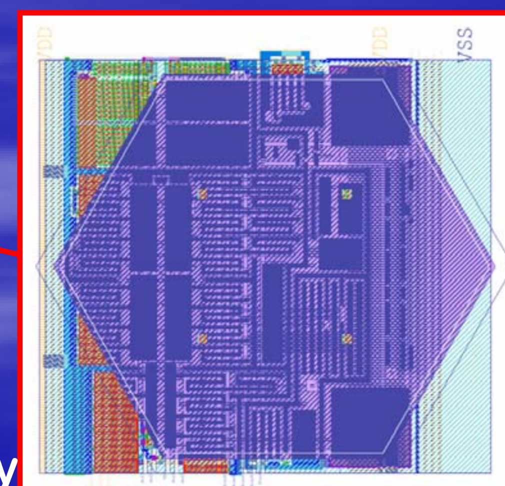

pixel electronics dimension:
80 μm x 80 μm in an hexagonal array, comprehensive of preamplifier/shaper, S/H and routing (serial read-out) for each pixel
number of pixels: 2101

~3.5 μs shaping time
100 e- ENC
100 mv/fC input sensitivity
20 fC dynamic range

Tracks reconstruction

1) The track is recorded by the PIXel Imager

2) Baricenter evaluation

3) Reconstruction of the principal axis of the track: maximization of the second moment of charge distribution

4) Reconstruction of the conversion point: major second moment (track length) + third moment along the principal axis (asymmetry of charge release)

5) Reconstruction of emission direction: pixels are weighted according to the distance from conversion point.

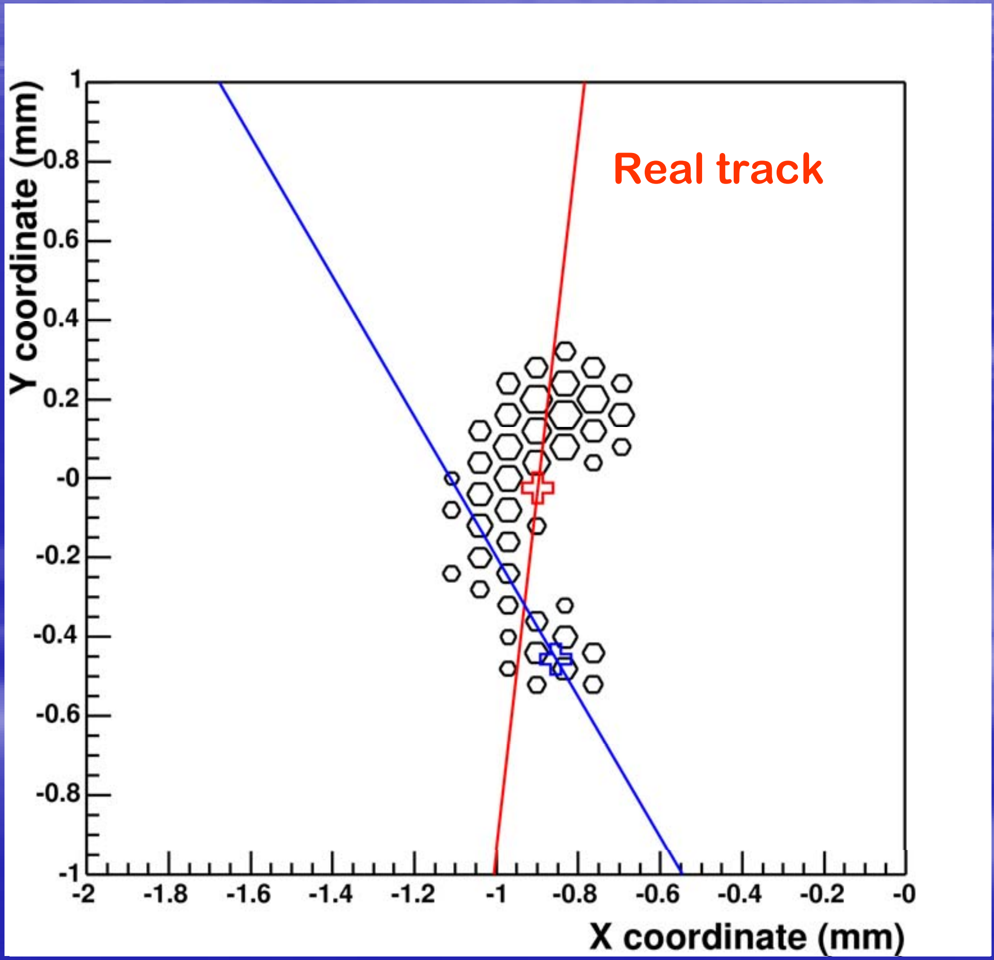

From 2k to 22k pixels

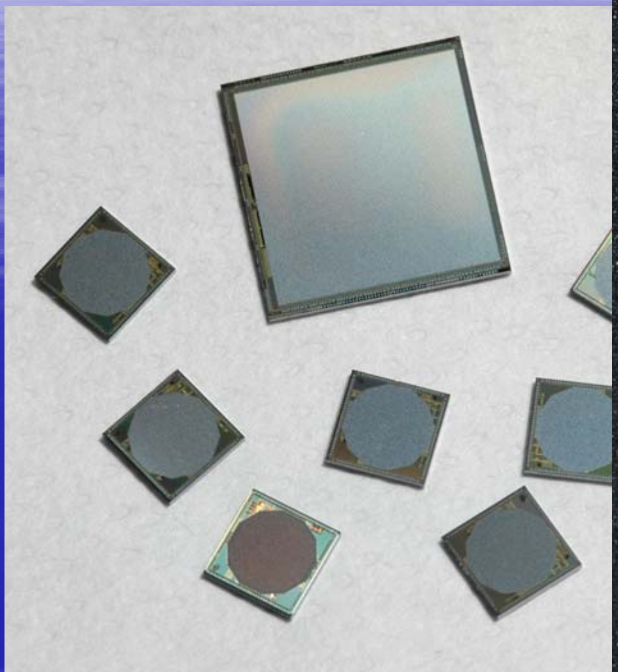

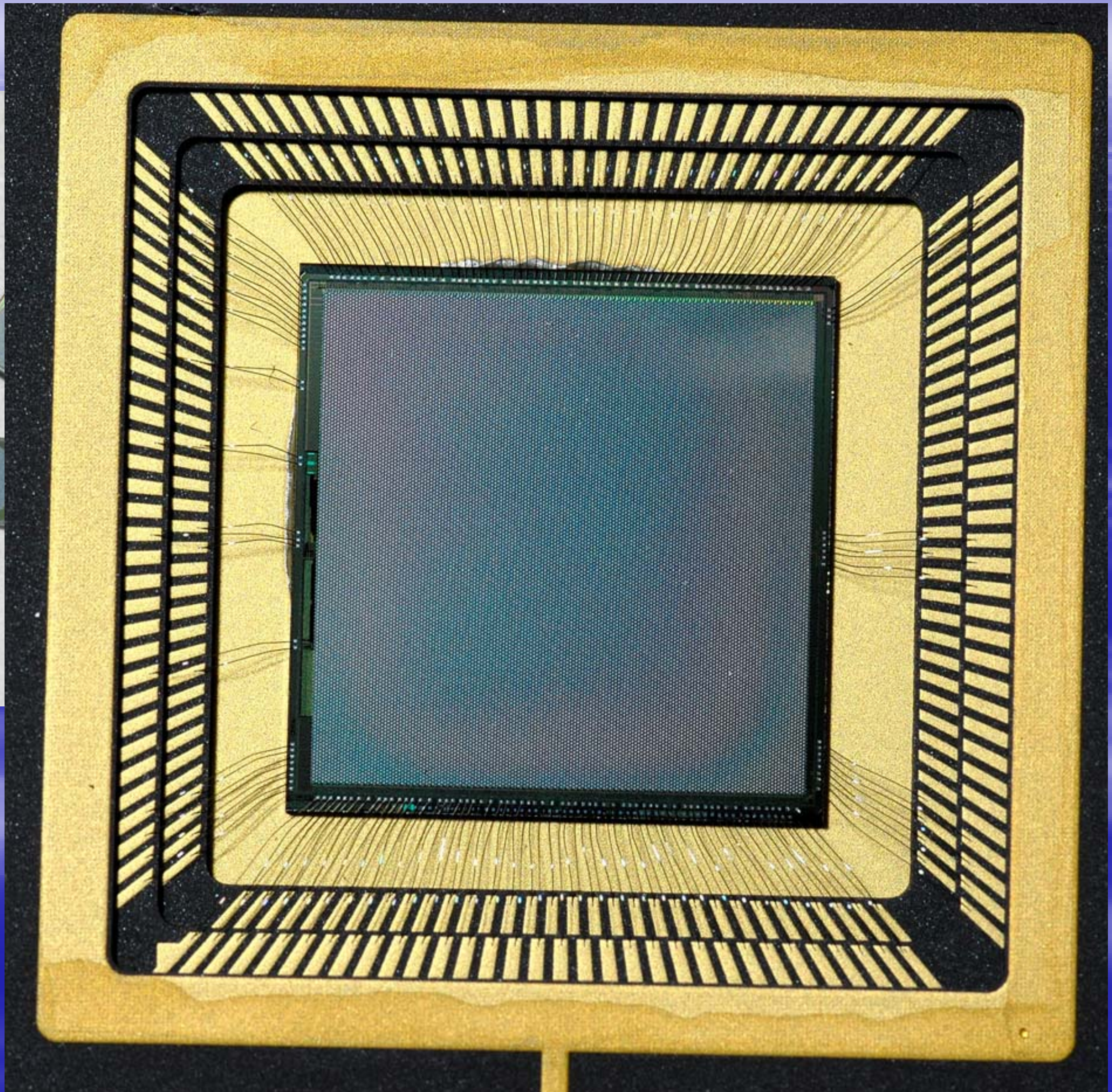

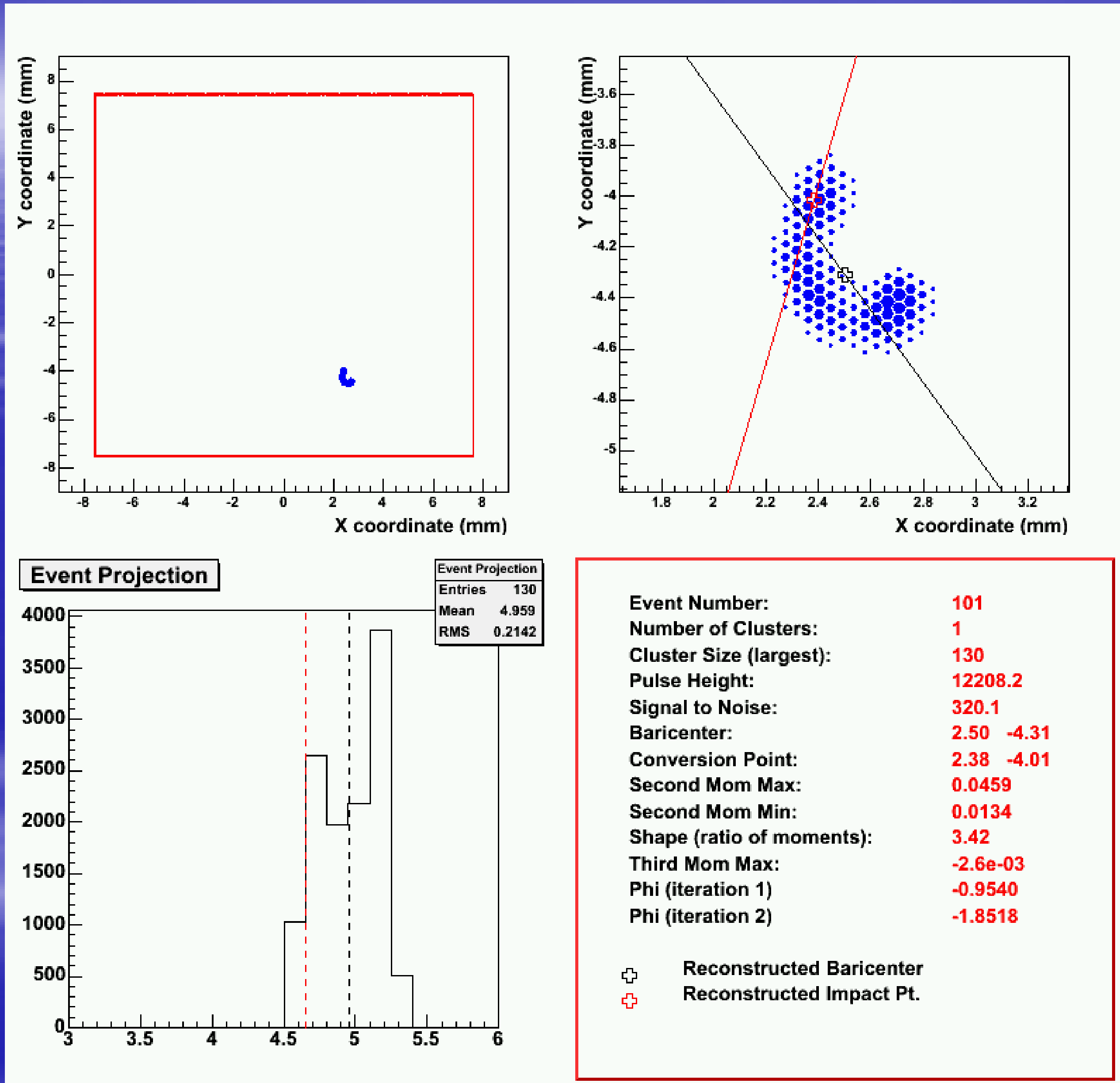
Y coordinate (mm)
X coordinate (mm)
Y coordinate (mm)
X coordinate (mm)
Event Projection
Event Projection
Entries 130
Mean 4.959
RMS 0.2142
Event Number: 101
Number of Clusters: 1
Cluster Size (largest): 130
Pulse Height: 12208.2
Signal to Noise: 320.1
Baricenter: 2.50 -4.31
Conversion Point: 2.38 -4.01
Second Mom Max: 0.0459
Second Mom Min: 0.0134
Shape (ratio of moments): 3.42
Third Mom Max: -2.6e-03
Phi (iteration 1) -0.9540
Phi (iteration 2) -1.8518
Reconstructed Baricenter
Reconstructed Impact Pt.

Further technological step: a 0.18 μm CMOS VLSI

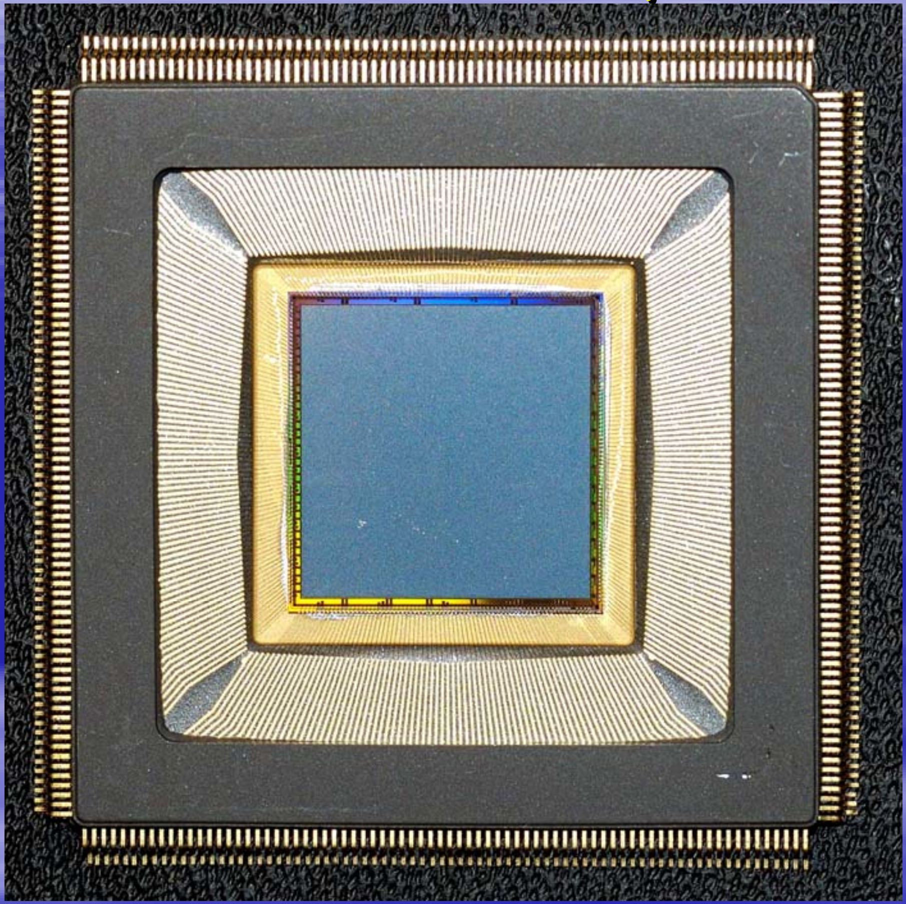

The chip integrates more than 16.5 million transistors.
It has a15mm x 15mm active area of 105’600 pixels organized in a honeycomb matrix

470 pixels/mm^2

Matrix organization

300 (width=300x50μm=15mm) x 352 (height=352x43.3μm=15.24mm) pixels
16 clusters of 300 x 22 = 6600 pixels each or
8 clusters of 300 x 44 = 13200 pixels each

0.18 μm ASIC features

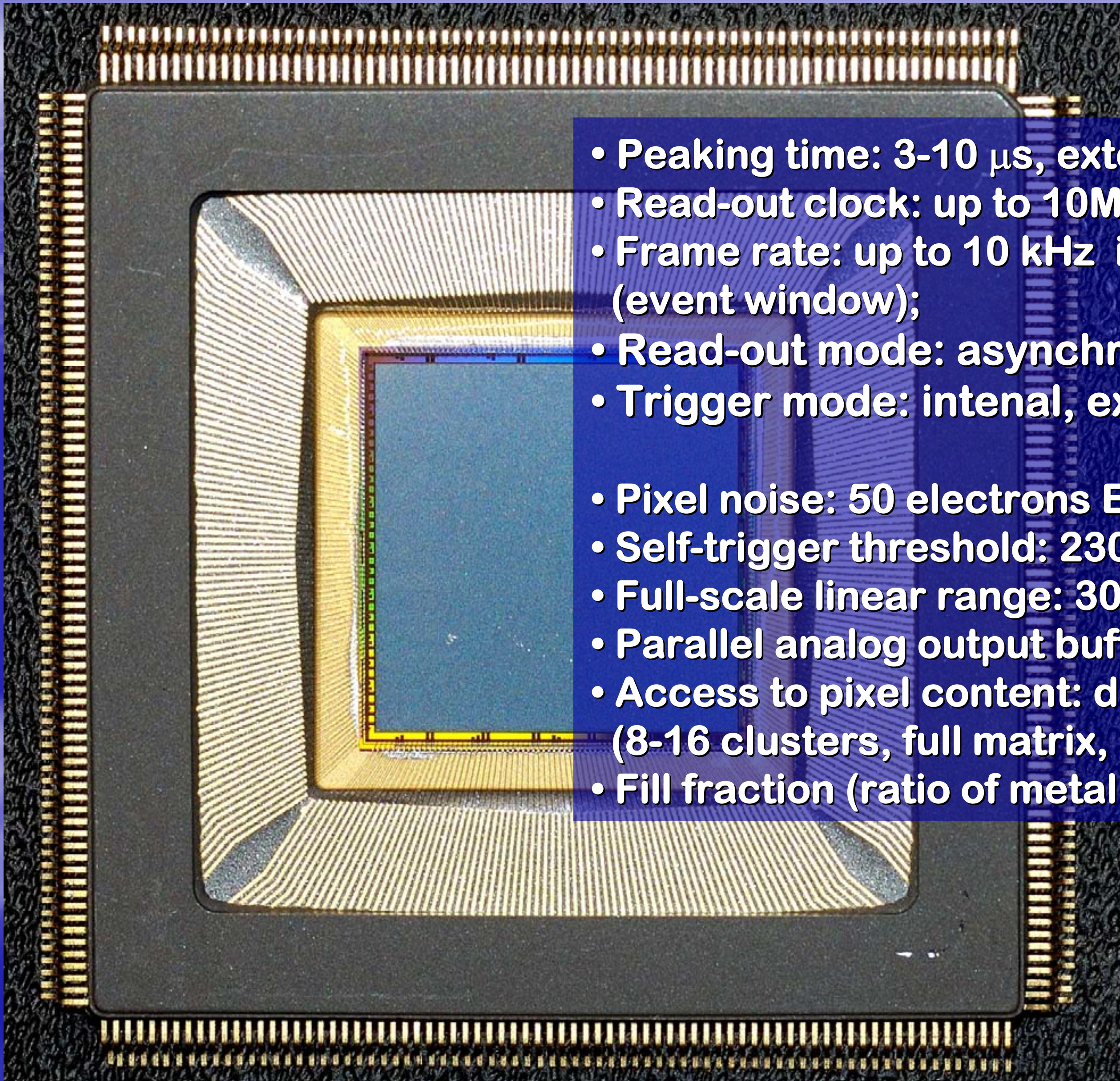

- Peaking time: 3-10 μs, externally adjustable;
- Read-out clock: up to 10MHz;
- Frame rate: up to 10 kHz in self-trigger mode (event window);
- Read-out mode: asynchronous or synchronous;
- Trigger mode: intenal, external or self-trigger;

- Pixel noise: 50 electrons ENC;
- Self-trigger threshold: 2300 electrons;
- Full-scale linear range: 30000 electrons;
- Parallel analog output buffers: 1, 8 or 16;
- Access to pixel content: direct (single pixel) or serial (8-16 clusters, full matrix, region of interest);
- Fill fraction (ratio of metal area to active area): 92%

Total power dissipation
~ 0.5 Watt

Self-trigger functionality

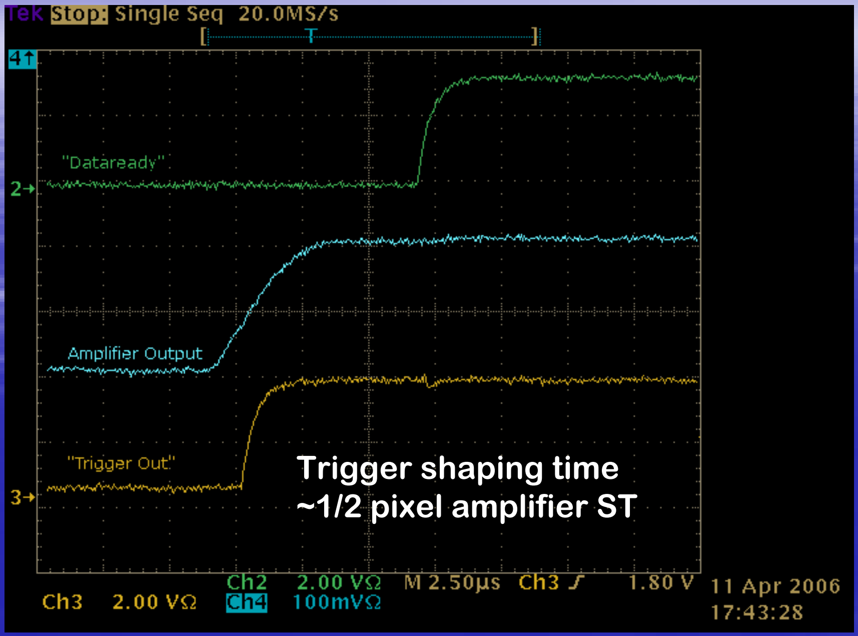

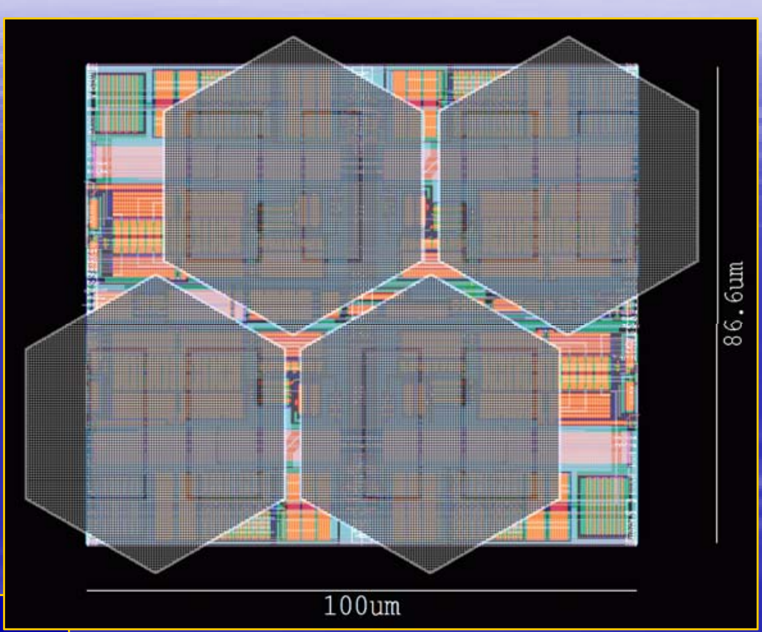

- ✓ charge sum of mini-cluster of 4 pixels contribute to a <u>local</u> trigger with dedicated s.a.
- ✓ threshold < 3000 e^- (10% FS)
- ✓ individual pixel trigger mask
- ✓ independent trigger level for each 16 clusters
- ✓ event localization in rectangle containing all triggered mini-clusters + user selectable region of 10 or 20 pixels
- ✓ the chip calculates the event ROI ($X_{min}, Y_{min} - X_{max}, Y_{max}$) for subsequent sequential readout of selected area

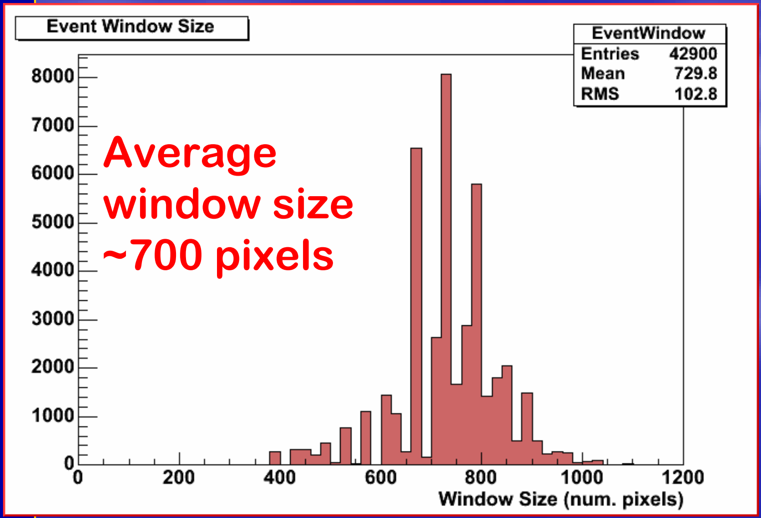

Noise and threshold

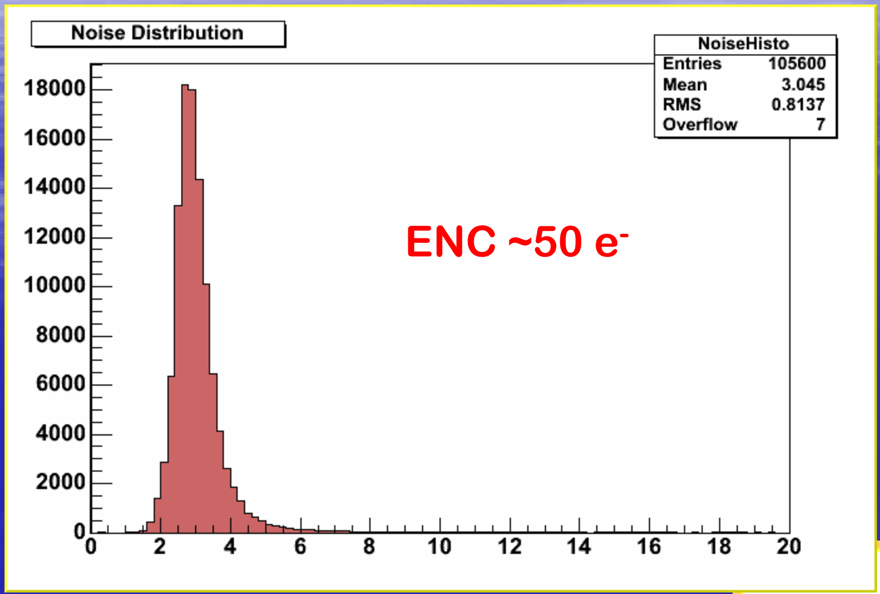

Self-trigger threshold constrained by pedestal offset more than pedestal fluctuations

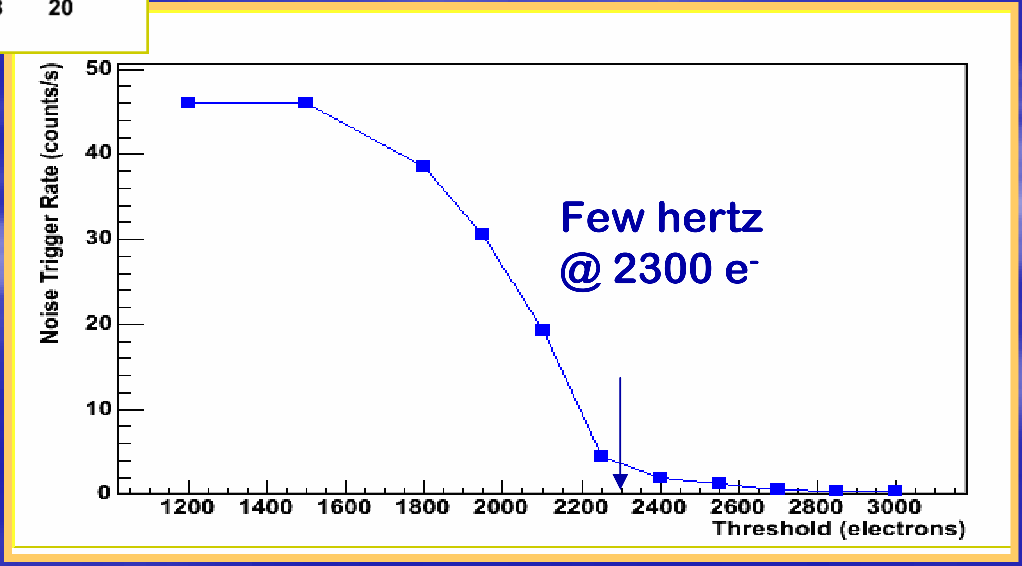

Detector assembly

- GEM pitch: 50 μm
- GEM holes diameters: 33 μm, 15 μm
- Read out pitch: 50 μm
- Absorption gap thickness: 10 mm
- Collection gap thickness: 1 mm

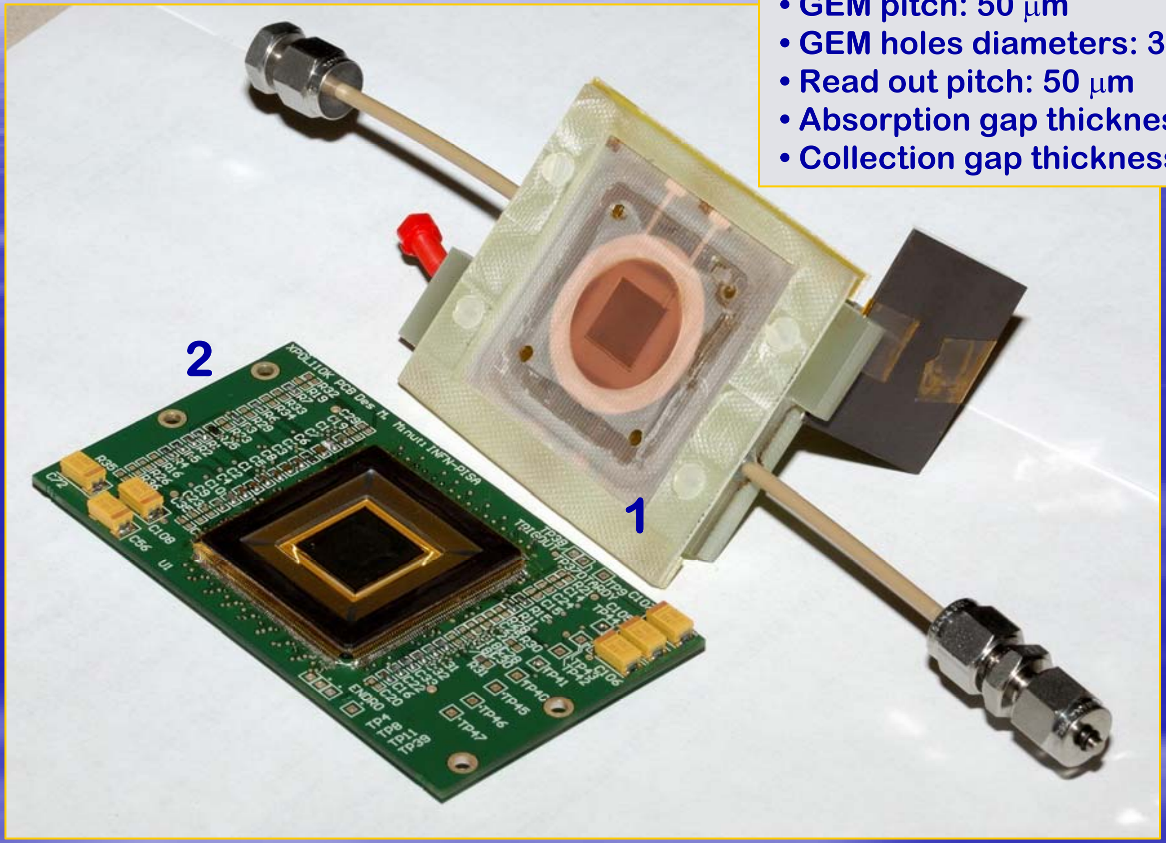

1 - The GEM glued to the bottom of the gas-tight enclosure
2 - The large area ASIC mounted on the control motherboard

Large effective gas gain around 1000 @450V in Ne(50%)-DME(50%)
(at least 70 V less than in our standard 90 μm pitch GEM)

GEM specs

pitch: 50 µm

holes outer Ø: 35 µm

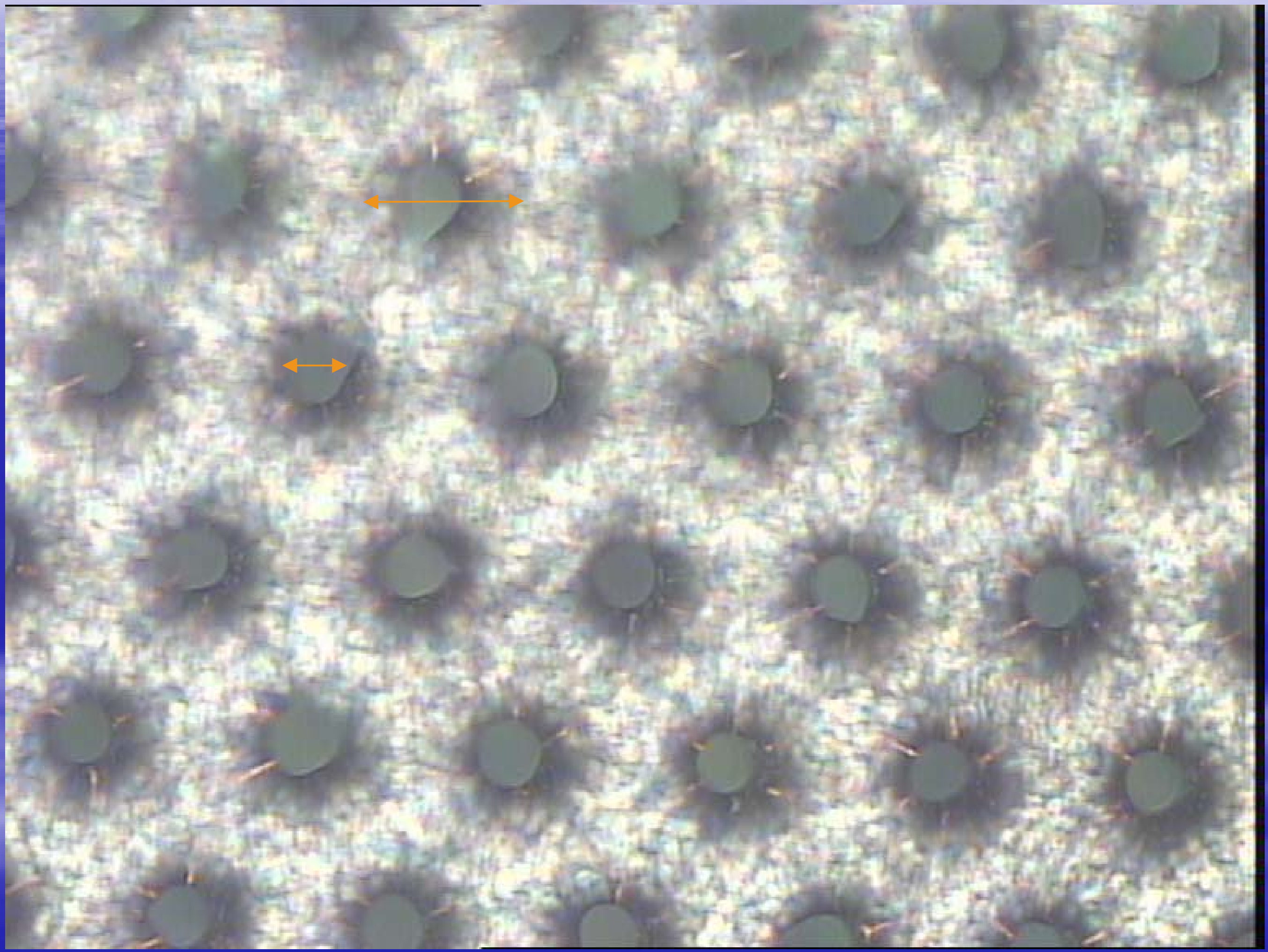

The matching of readout and gas amplification (GEM) pitch allows getting optimal results and to fully exploit the very high granularity of the device

The read-out system

On-line monitoring

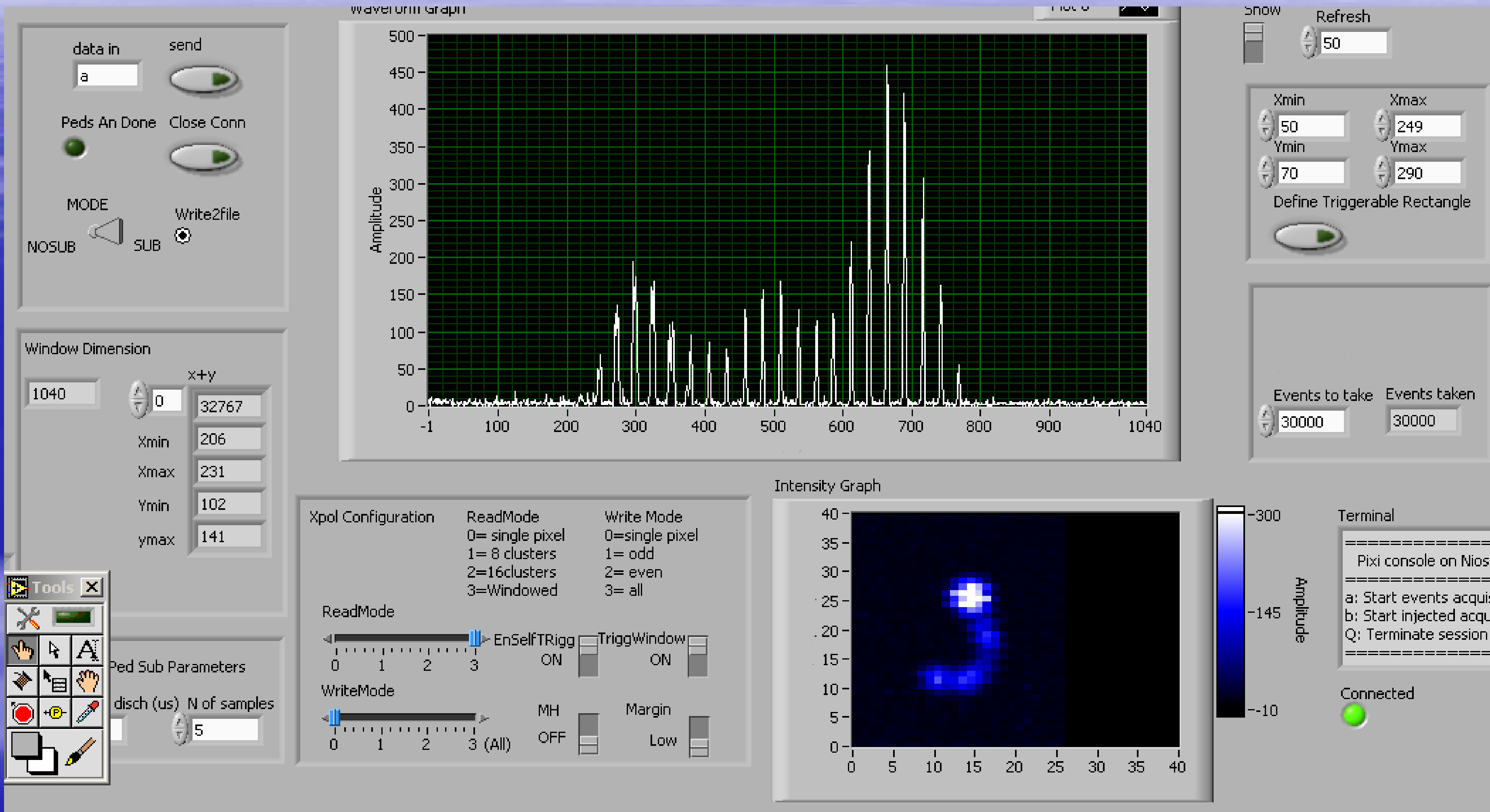

Real time pedestal subtraction

Imaging capability

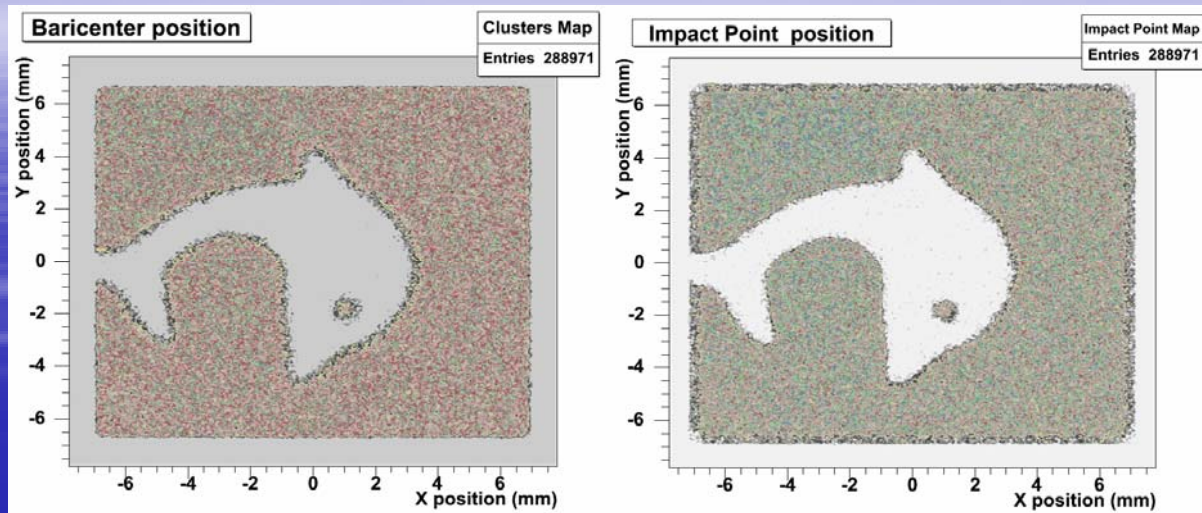

^{55}Fe source **Ne(50%)-DME(50%)**

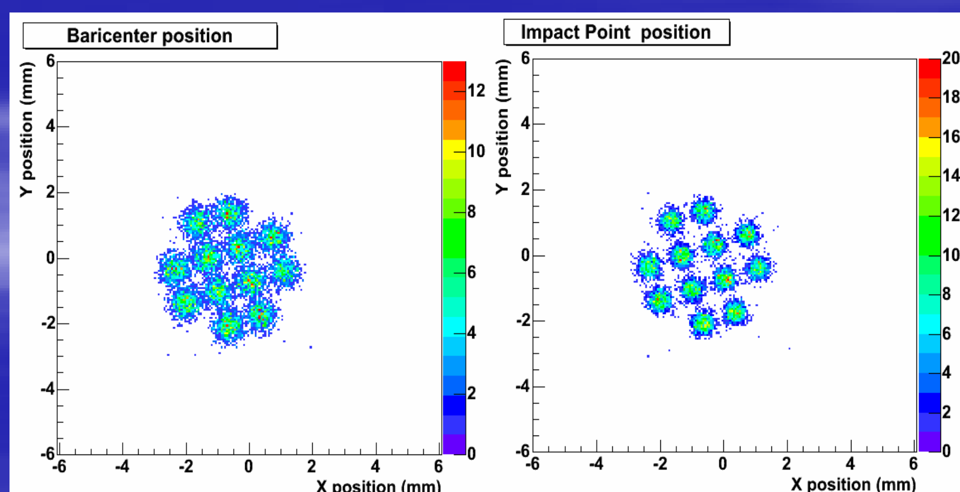

Holes: 0.6 mm diameter, 2 mm apart.

Imaging and spectroscopic capability

Argon (50%)-DME(50%)

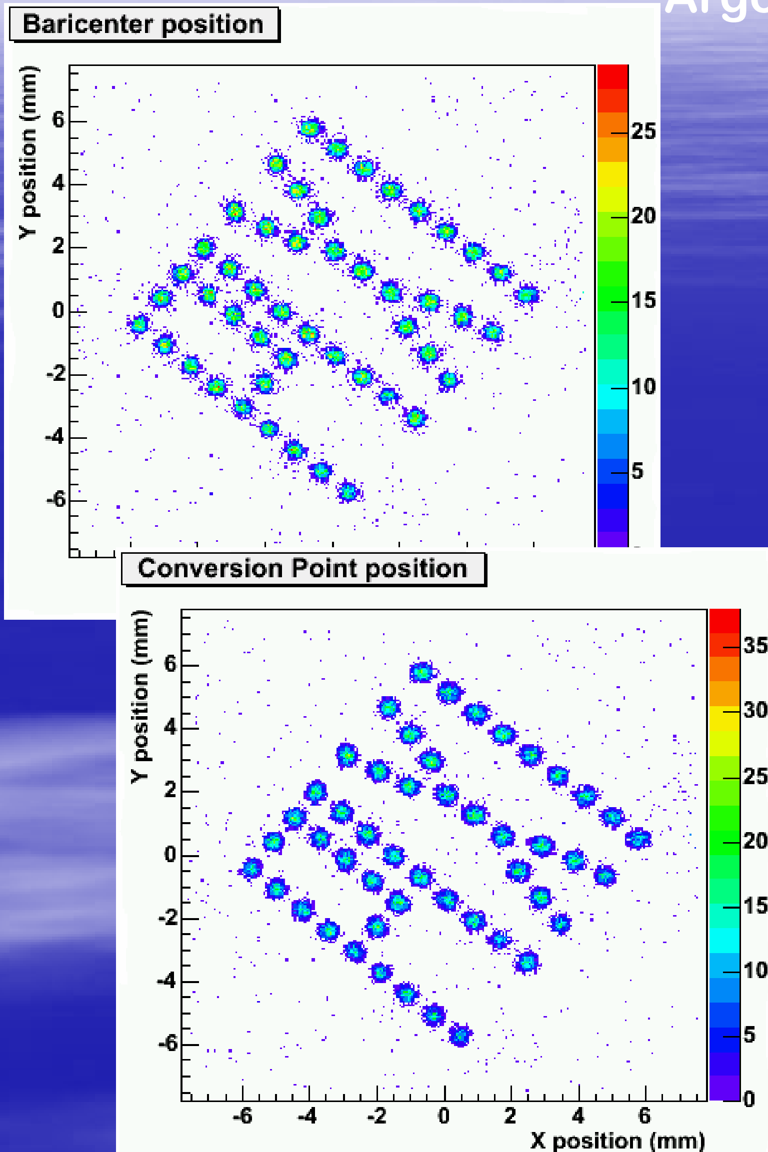

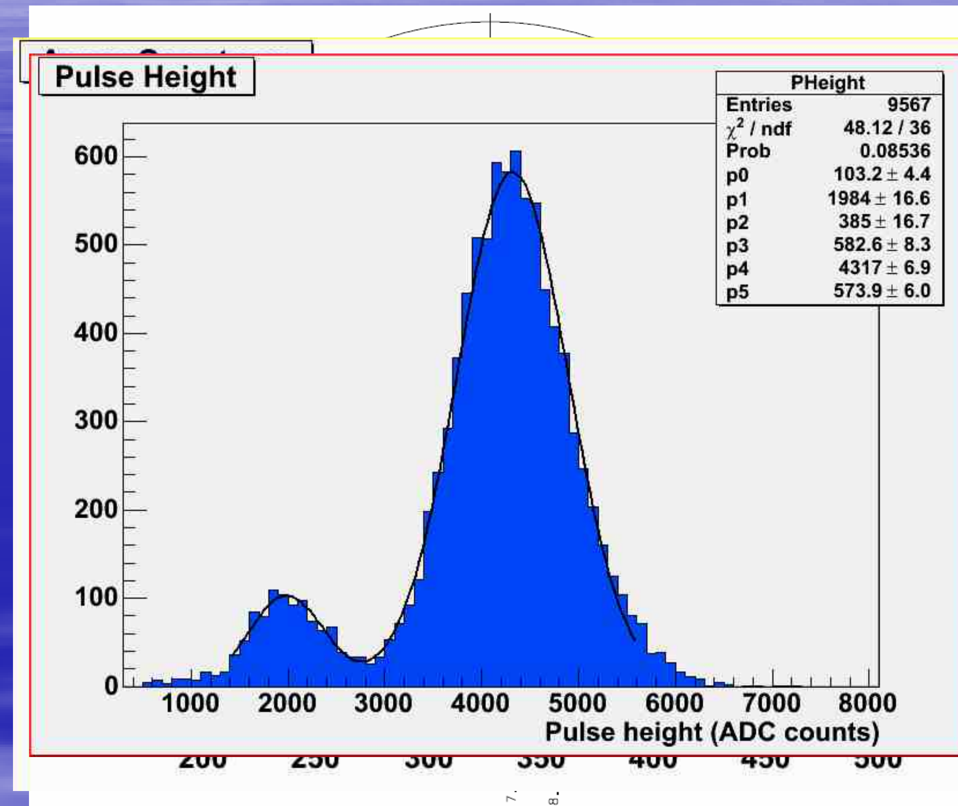

Holes:
Ø 0.5 mm
pitch 1 mm

Polarizing X-rays

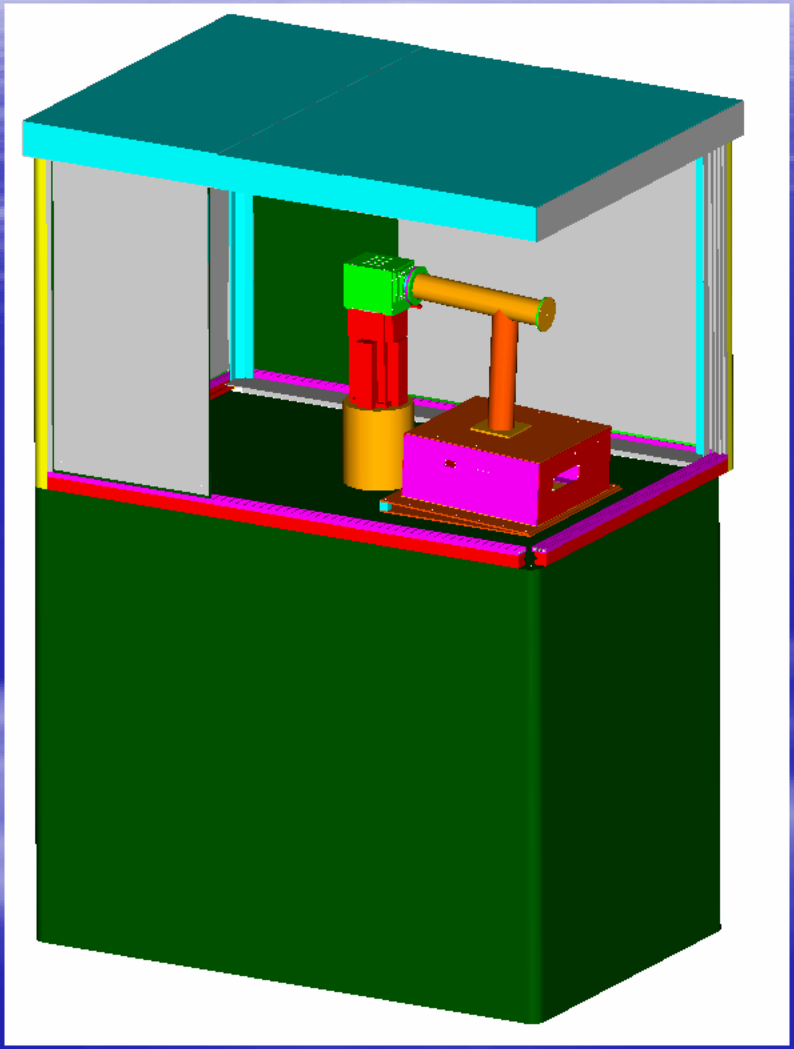

90° Thompson scattering

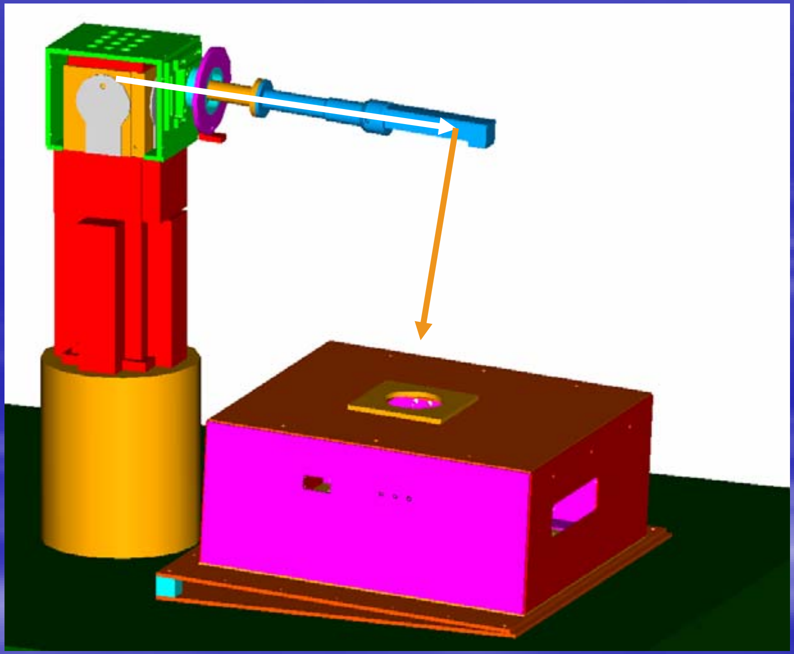

Track morphology and angle reconstruction

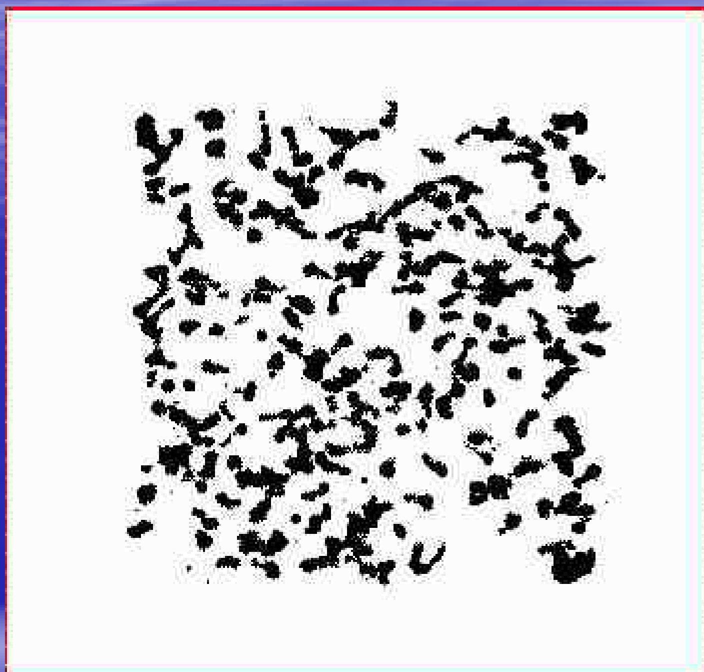

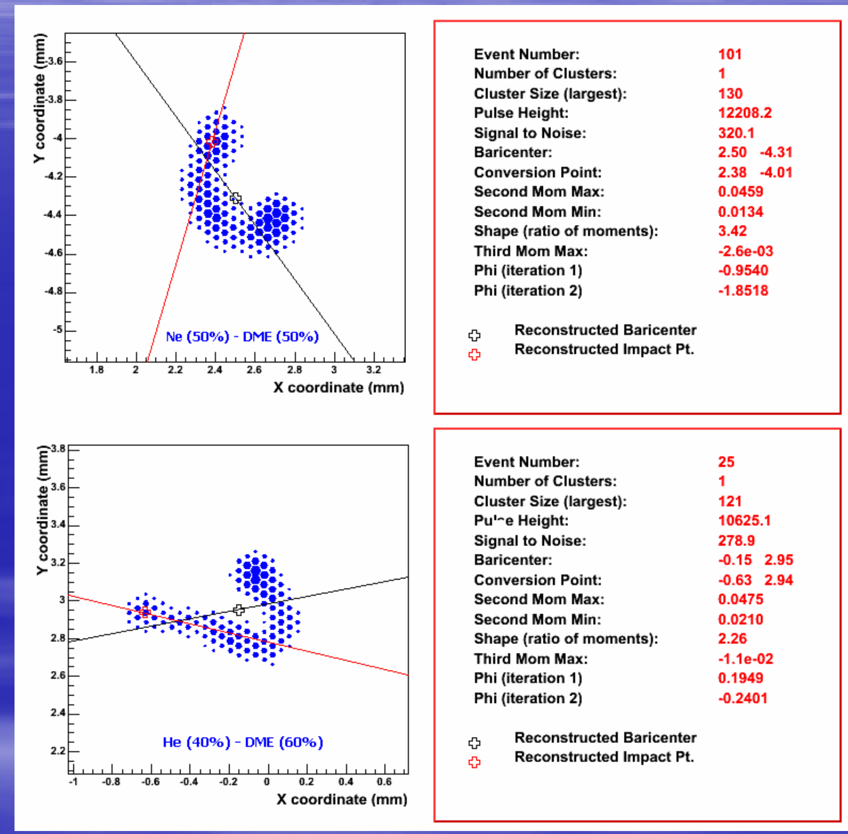

Modulation factor

Measured with two different gas mixtures:
He/DME and Ne/DME

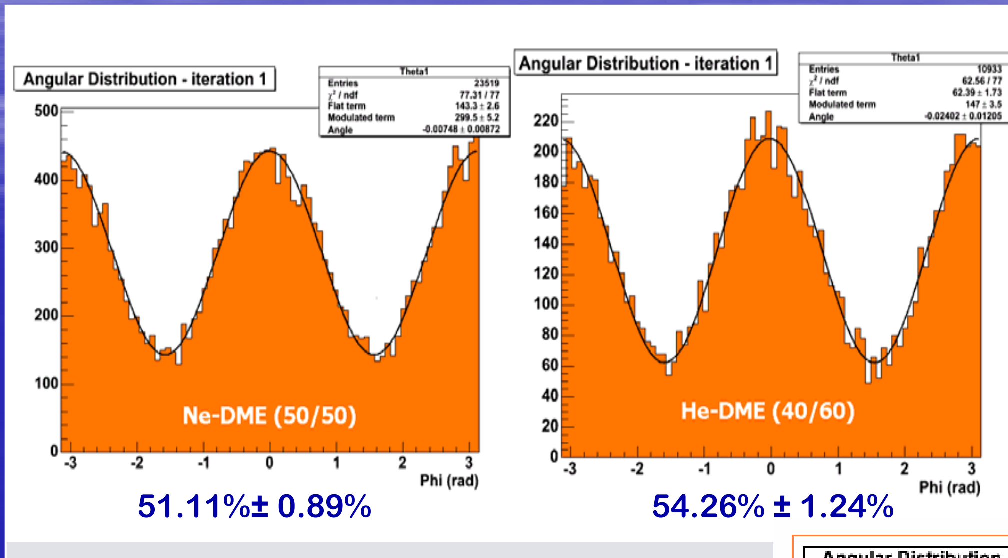

@5.4 keV Cr-line energy

@6.4 keV Fe energy

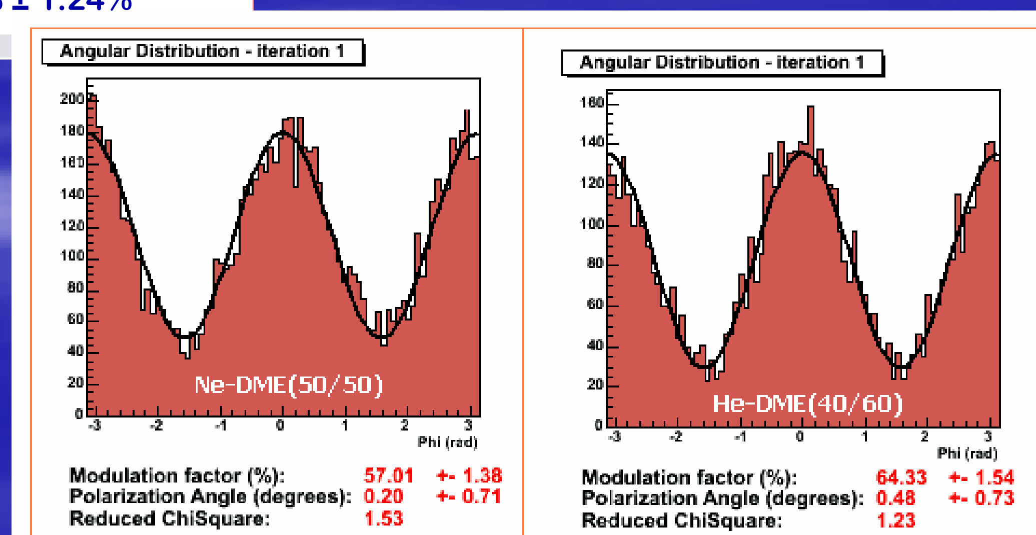

Residual modulation

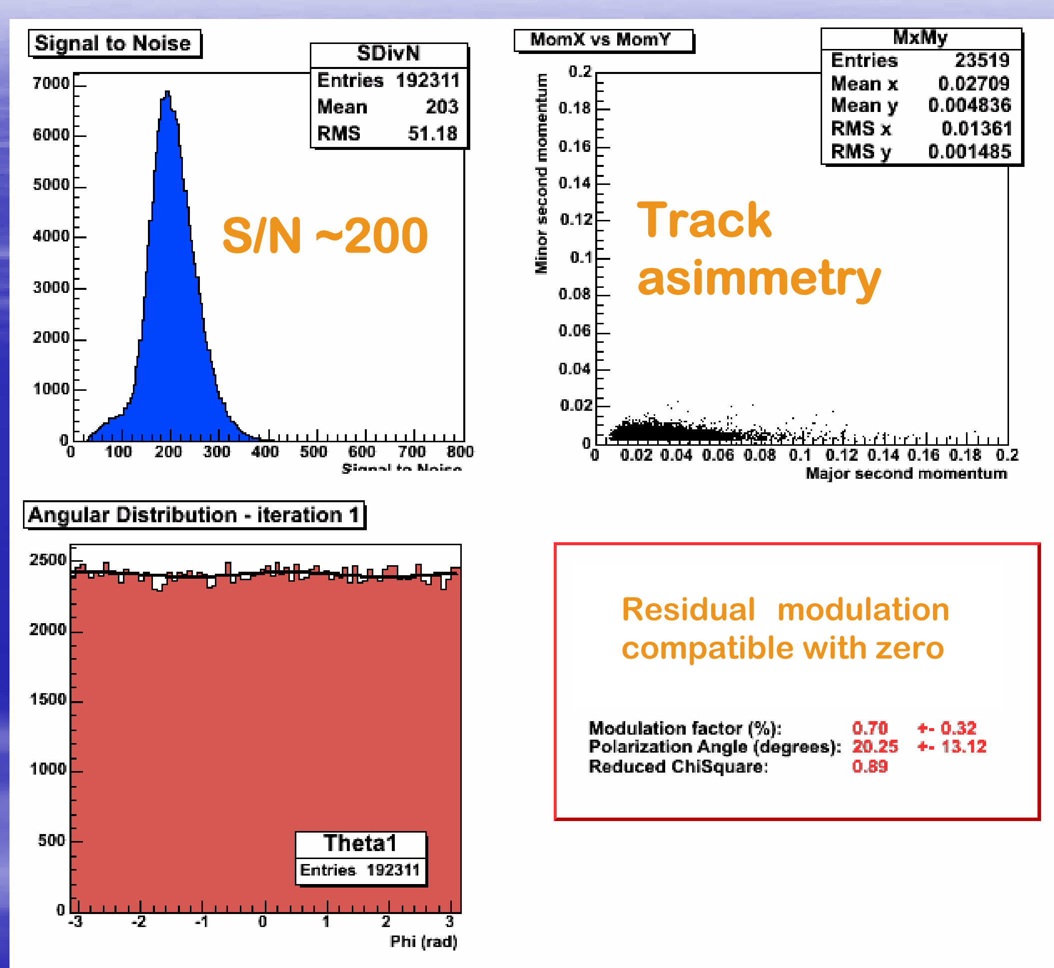

S/N distribution, scatter plot of the two principal axes of the cluster charge and residual modulation, obtained with ^{55}Fe source in Ne(50%)-DME(50%)

Expected MDP with XEUS optics
@ different source fluxes and spectral index

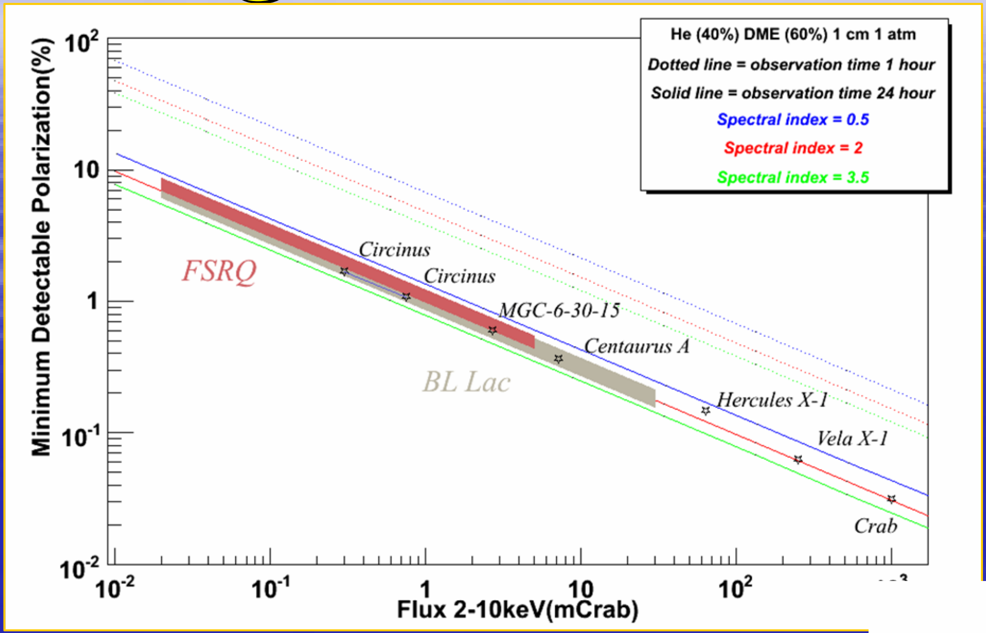

He(40%)-DME(60%)

With observations of one day we can measure the polarization of several AGNs down to 1 % for 1 mCrab flux

With 1 h it is possible to get few % with a 10 mCrab flux

Ne(50%)-DME(50%)

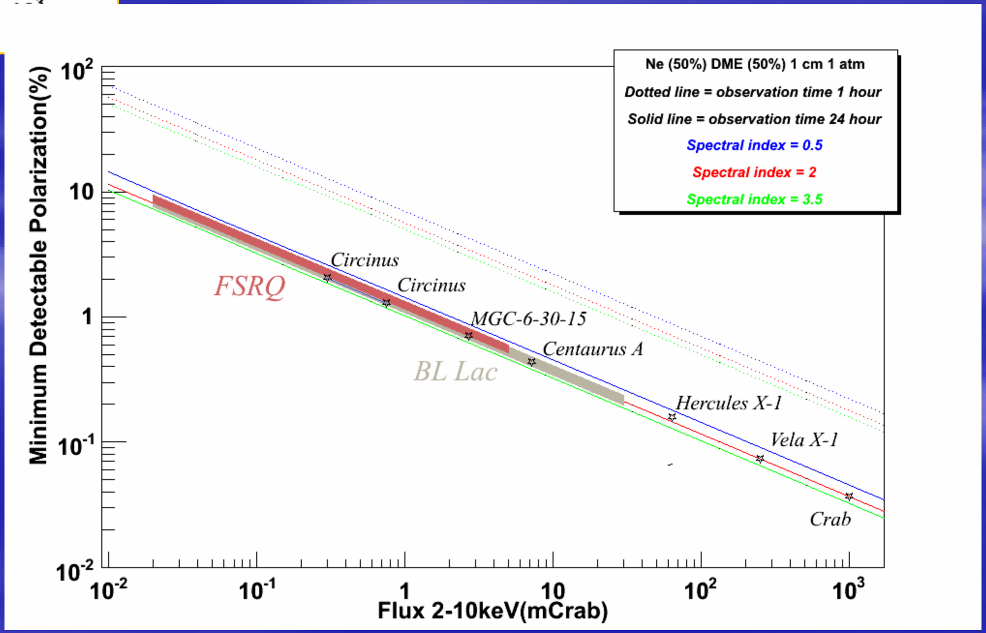

Conclusions

With devices like the one presented the class of Gas Pixel Detectors has reached the level of integration, compactness and resolving power typical of solid state detectors.

Depending on type of electron multiplier, pixel and die size, electronics shaping time, analog vs. digital read-out, counting vs. integrating mode, many applications can be envisaged for this class of detectors.

As for the X-ray polarimetry applications a residual modulation very low and a modulation factor well above 50% will likely allow polarimetric measurements at the level of ~1% for hundreds of galactic and extragalactic sources.

A real breakthrough in X-ray astronomy
if compared with the traditional X-ray polarimeters sensitivity.

Table 1 Physical characteristics and performances of the micro-pattern detector

	Present prototype (2–10 keV)	Improved configuration (3.5–10 keV)
Drift/absorption gap	6 mm	30 mm
Drift field	3,000 V cm^{-1}	1,500 V cm^{-1}
Gas filling and pressure	(Ne 80%–DME 20%); 1 atm	(Ne 40%–DME 60%); 4 atm
Gas grain	5,000	2,500
Transverse diffusion in drift	80 μm	<100 μm
GEM thickness	50-μm copper-clad kapton foil	50-μm copper-clad kapton foil
GEM hole geometry	40-μm diameter; 60-μm pitch	40-μm diameter; 60-μm pitch
GEM voltage	400 V	600 V
Detection efficiency at 5.4 keV		
Read-out pixel size		
Number of pixels		
Read-out plane technology		
Track length/pixel size (6 keV)		
Sensitivity to Her X1		= 10%
Sensitivity to 3C-273		DP = 1%
Sensitivity to MCG-6-30-15		DP = 1%
Gain in the integration time over S		)0 (over Bragg)
Gain in the integration time over S		000 (over Bragg)

letters to nature

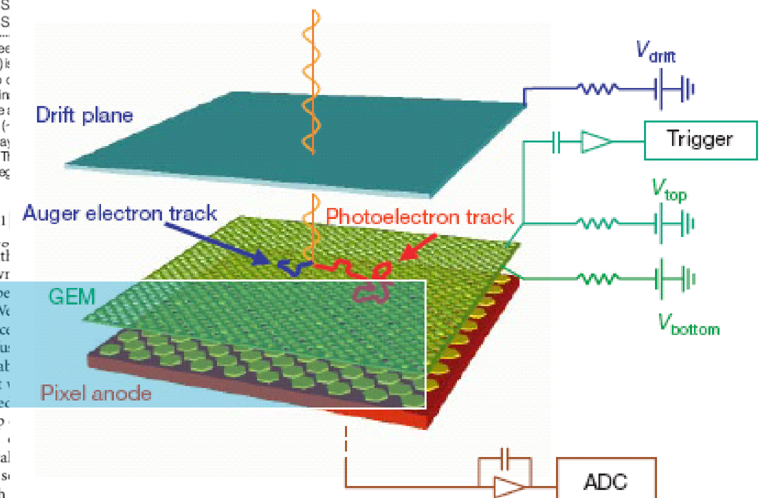

The MPGC requires integration periods that are about 100 times shorter than those of the SXRP to detect the same polarization in bright sources. With integrations of the order of one day we could perform polarimetry of active galactic nuclei at the 1% level, a breakthrough in this fascinating window of high-energy astrophy-

L122 (1978).
20. Kaaret, P. et al. SXRP: a focal plane stellar X-ray polarimeter for the Spectrum-X-Gamma mission. *Opt. Eng.* 29, 773–783 (1990).
21. Schnopper, H. W. & Kalata, K. Polarimeter for celestial X-rays. *Astron. J.* 74, 854–858 (1969).
22. Novick, R. in *Planets, Stars and Nebulae Studied with Photopolarimetry* (ed. Gerehls, T.) 262–317 (Univ. Arizona Press, Tucson, 1972).

28. Austin, R. A., Minamitani, T. & Ramsey, B. Development of a hard X-ray imaging polarimeter. *Proc. SPIE* 2010, 118–125 (1993).
29. La Monaca, A. *et al.* A new photoelectron imager for X-ray astronomical polarimetry. *Nucl. Instrum. Methods A* 416, 267–277 (1998).
30. Sauli, F. GEM: a new concept for electron amplification in gas detectors. *Nucl. Instrum. Methods A* 386, 531–534 (1997).
31. Campbell, M. *et al.* A pixel readout chip for 10–30 Mrad in standard 0.25 μm CMOS. *IEEE Trans. Nucl. Sci.* 46, 156–160 (1999).
32. Bavdaz, M. *et al.* Status of the X-ray evolving universe spectroscopy mission (XEUS). *Proc. SPIE* 4138, 69–78 (2000).
33. Christensen, F. E. *et al.* X-ray calibration of the SODART flight telescope. *Proc. SPIE* 3113, 69–78 (1997).

An efficient photoelectric X-ray polarimeter for the study of black holes and neutron stars

E. Costa, P. Soffitta, R. Bellazzini, A. Brez, N. Lumb, G. Spandre

Nature, Vol. 411 (2001) 662.